

DiffProtect: Generate Adversarial Examples with Diffusion Models for Facial Privacy Protection

Jiang Liu¹, Chun Pong Lau², Zhongliang Guo³, Yuxiang Guo¹, Zhaoyang Wang¹, Rama Chellappa¹

¹Johns Hopkins University, ²City University of Hong Kong, ³University of St Andrews

Abstract

The increasingly pervasive facial recognition (FR) systems raise serious concerns about personal privacy, especially for billions of users who have publicly shared their photos on social media. Several attempts have been made to protect individuals from being identified by unauthorized FR systems utilizing adversarial attacks to generate encrypted face images. However, existing methods suffer from poor visual quality or low attack success rates, which limit their utility. Recently, diffusion models have achieved tremendous success in image generation. In this work, we ask: can diffusion models be used to generate adversarial examples to improve both visual quality and attack performance? We propose DiffProtect, which utilizes a diffusion autoencoder to generate semantically meaningful perturbations on FR systems. Extensive experiments demonstrate that DiffProtect produces more natural-looking encrypted images than state-of-the-art methods while achieving significantly higher attack success rates, e.g., 24.5% and 25.1% absolute improvements on the CelebA-HQ and FFHQ datasets.

1. Introduction

The rise of deep neural networks has enabled the tremendous success of facial recognition (FR) systems [5, 43, 15]. However, the widely deployed FR systems also pose a huge threat to personal privacy as billions of users have publicly shared their photos on social media. Through large-scale social media photo analysis, FR systems can be used for detecting user relationships [46], stalking victims [47], stealing identities [32], and performing massive government surveillance [42, 17, 34]. It is urgent to develop facial privacy protection techniques to protect individuals from unauthorized FR systems.

Recently, several works [3, 58, 20] proposed to use adversarial attacks to generate encrypted face images and protect users from being identified by FR systems. However, existing attacks on FR systems [3, 20, 27, 45, 59, 58, 61] often suffer from poor visual quality, especially noise-based [3, 58] (Fig. 1a) and patch-based methods [27, 45]

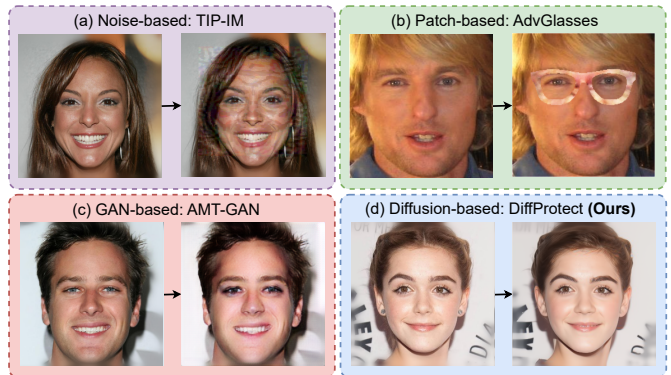


Figure 1: Illustration of different face encryption methods [58, 20, 45]. The proposed DiffProtect produces natural and imperceptible changes to the input images while achieving competitive attack success rates.

(Fig. 1b), which add unnatural and conspicuous changes to the source images. From a user-centered perspective, these approaches are not desirable in practice, as everyone wants to post their best-looking photos on social media – not unattractive photos, even though they might be encrypted for protecting personal privacy.

An ideal facial identity encryption algorithm should only create *natural* or *imperceptible* changes to the source images. To achieve this goal, several works [59, 20, 38, 4] attempted to generate natural-looking adversarial examples using generative adversarial networks (GANs) [10, 25] by transferring make-up styles [59, 20] or editing facial attributes [38, 22]. Although these works have demonstrated promising results, the attack success rates (ASRs) of GAN-based methods can be lower than noise-based and patch-based methods since the output images are constrained on the learned manifold of a GAN. Moreover, most of the GAN-based facial encryption methods [20, 59] require training the model with a fixed victim identity. In other words, these models are target specific and we need to re-train the model when the target identity is changed. In addition, the visual quality of images generated by GAN-based methods is still dissatisfying (see Fig. 1c).

Recently, diffusion models [18, 51, 50, 37, 24] have emerged as state-of-the-art generative models that are capable of synthesizing realistic and high-resolution images. It has been shown that diffusion models perform better than GANs on many image generation tasks [6, 40, 37] and maintain better coverage of the image distribution [6]. With the rise of diffusion models, a natural question arises: *can we utilize diffusion models as better generative models to generate adversarial examples with both high attack success rates and high visual quality?* It has been shown that diffusion models can improve adversarial robustness [12, 39, 54, 36, 1]. However, whether the strong generative capacity of diffusion models can be used to generate adversarial attacks has not been explored.

To this end, we propose DiffProtect, which utilizes a pre-trained diffusion autoencoder [37] to generate adversarial images for facial privacy protection. The overall pipeline of DiffProtect is shown in Fig. 2. We first encode an input face image \mathbf{I} into a high-level semantic code \mathbf{z} and a low-level noise code \mathbf{x}_T . We then iteratively optimize an adversarial semantic code \mathbf{z}_{adv} such that the resulting protected image \mathbf{I}_p generated by the conditional DDIM decoding process [37, 50] can fool the face recognition model. In this way, we can create semantically meaningful perturbation to the input image and utilize a diffusion model to generate high-quality adversarial images (see Fig. 1d). We further introduce a face semantics regularization module to encourage that \mathbf{I}_p and \mathbf{I} share similar face semantics to better preserve visual identity. Our extensive experiments on the CelebA-HQ [23] and FFHQ [25] datasets show that DiffProtect produces protected face images of high visual quality, while achieving significantly higher ASRs than the previous best methods, *e.g.*, +24.5% absolute ASR on CelebA-HQ with IRSE50 [19] as the victim model.

One drawback of diffusion models is the slow generation process, which requires many evaluation steps to generate one image. This can be problematic since we need to iteratively optimize the semantic latent code. To address this issue, we propose an attack acceleration strategy that computes an approximated version of the reconstructed image at each attack iteration by running only one generative step, which drastically reduces the attack time while maintaining competitive attack performance.

Our main contributions are summarized as follows:

- We propose a novel diffusion model based attack method, termed DiffProtect, for facial privacy protection, which crafts natural and inconspicuous adversarial examples on face recognition systems.
- We further propose a face semantics regularization module to better preserve visual identity and a simple yet effective attack acceleration strategy to improve attack efficiency.

- Our extensive experiments on the CelebA-HQ and FFHQ datasets demonstrate that DiffProtect produces more natural-looking encrypted images than state-of-the-art methods while achieving competitive attack performance.

2. Related Work

Adversarial Attacks with Generative Models While most of the existing adversarial attacks focus on optimizing additive noises in the pixel space [11, 33, 2, 7], several works [55, 56, 21, 38, 59, 20] proposed to generate adversarial attacks with generative models, which produce perceptually realistic adversarial examples. Wong *et al.* [55] trained a conditional variational autoencoder (VAE) [49, 26] to generate a variety of perturbations and utilized the learned perturbation sets to improve model robustness and generalization. Xiao *et al.* [56] trained a conditional GAN to directly produce adversarial examples. [21, 31, 52] generate on-manifold adversarial examples by optimizing latent codes in the latent space of GANs. Qiu *et al.* [38] generated semantically realistic adversarial examples by attribute-conditioned image editing using a GAN. To the best of our knowledge, this is the first work that utilizes diffusion models for generating adversarial attacks.

Diffusion Models and Adversarial Robustness Diffusion models [48, 18, 35] are a family of generative models that model the target distribution by learning a reverse generative denoising process. Recently, diffusion models have become state-of-the-art methods that can synthesize more realistic and high-resolution images with more stable training process [18, 51, 50, 37, 24]. In the field of adversarial machine learning, it has been shown that diffusion models can help to improve adversarial robustness and achieve state-of-the-art results [12, 39, 54, 36, 1]. [12, 39, 54] used diffusion models to generate synthetic data for adversarial training. [36, 1] exploited pretrained diffusion models as purification modules that remove the adversarial noise in the input images for empirical [36] and certified [1] defenses. However, it remains unknown whether the strong generative capacity of diffusion models can be used to generate adversarial attacks and in this work we make the first attempt in this direction.

Adversarial Attacks on Face Recognition Many studies have been proposed to attack FR systems, including both poisoning [44] and evasion [3, 20, 27, 45, 59, 58] attacks. Poisoning attacks require injecting poisoned face images into the training sets of FR systems, which is unlikely to achieve for individual users. Evasion attacks, especially transferable black-box attacks, are more practical for protecting facial image privacy, as they only require perturbing

the source images to fool the FR systems at test time. Existing attacks on FR systems [3, 20, 27, 45, 59, 58] suffer from poor visual quality or low attack success rates, which limit their usability in the real world. Noise-based methods such as Lowkey [3] and TIP-IM [58] create unexplainable noise patterns on face images. Patch-based methods such as Adv-Hat [27] and Adv-Glasses [45] add unnatural and conspicuous patches to the source images. GAN-based methods generate more natural-looking adversarial examples [59, 20, 38, 22], but typically have lower attack success rates. In addition, [59, 20] drastically change the makeup styles of source images and might be biased towards female users [20]. In contrast, the proposed DiffProtect creates natural and imperceptible changes to the source images and achieves competitive attack performance.

3. Background: Diffusion Models

Diffusion models [48, 18, 35] are a family of generative models that model the target distribution by learning a reverse denoising generative process. A diffusion model consists of two processes: (1) a forward diffusion process that converts the input image \mathbf{x}_0 to noise map \mathbf{x}_T by gradually adding noise in T forward steps; (2) a reverse denoising generative process that aims to recover \mathbf{x}_0 from \mathbf{x}_T by gradually denoising in T reverse steps.

A Gaussian diffusion process gradually adds Gaussian noise to the data in the forward diffusion process:

$$q(\mathbf{x}_t|\mathbf{x}_{t-1}) = \mathcal{N}(\sqrt{1 - \beta_t}\mathbf{x}_{t-1}, \beta_t\mathbf{I}), \quad (1)$$

where β_t ($t = 1, \dots, T$) are hyperparameters controlling the noise level at each diffusion step t . In the Gaussian diffusion process, the noisy image \mathbf{x}_t also follows a Gaussian distribution given \mathbf{x}_0 :

$$q(\mathbf{x}_t|\mathbf{x}_0) = \mathcal{N}(\sqrt{\alpha_t}\mathbf{x}_0, (1 - \alpha_t)\mathbf{I}), \quad (2)$$

where $\alpha_t = \prod_{s=1}^t (1 - \beta_s)$. The goal of a diffusion model is to learn the reverse distribution $p(\mathbf{x}_{t-1}|\mathbf{x}_t)$ so that we can generate data by sampling noise map \mathbf{x}_T from a prior distribution, *e.g.*, $\mathcal{N}(\mathbf{0}, \mathbf{I})$. When the difference between $t - 1$ and t is infinitesimally small, *i.e.*, $T = \infty$, $p(\mathbf{x}_{t-1}|\mathbf{x}_t)$ can be modeled as [48, 18]:

$$p(\mathbf{x}_{t-1}|\mathbf{x}_t) = \mathcal{N}(\mu_\theta(\mathbf{x}_t, t), \sigma_t^2\mathbf{I}), \quad (3)$$

where μ_θ is a neural network that predicts the posterior mean given the noisy image \mathbf{x}_t and time step t . In practice, Ho *et al.* [18] proposed to train a U-Net [41] to learn a function $\epsilon_\theta(\mathbf{x}_t, t)$ the noise that has been added to \mathbf{x}_0 by the following reweighted loss function:

$$\mathcal{L}_{\text{simple}} = \sum_{t=1}^T \mathbb{E}_{\mathbf{x}_0, \epsilon_t} \left[\|\epsilon_t - \epsilon_\theta(\mathbf{x}_t, t)\|^2 \right], \quad (4)$$

where ϵ_t is the ground-truth noise added to \mathbf{x}_0 to produce

\mathbf{x}_t . And $\mu_\theta(\mathbf{x}_t, t)$ can be obtained by:

$$\mu_\theta(\mathbf{x}_t, t) = \frac{1}{\sqrt{1 - \beta_t}} \left(\mathbf{x}_t - \frac{\beta_t}{\sqrt{1 - \alpha_t}} \epsilon_\theta(\mathbf{x}_t, t) \right). \quad (5)$$

Song *et al.* [50] proposed Denoising Diffusion Implicit Model (DDIM) that enjoys a deterministic generative process. DDIM has a non-Markovian forward process:

$$q(\mathbf{x}_{t-1}|\mathbf{x}_t, \mathbf{x}_0) = \mathcal{N}\left(\sqrt{\alpha_{t-1}}\mathbf{x}_0 + \sqrt{1 - \alpha_{t-1}} \frac{\mathbf{x}_t - \sqrt{\alpha_t}\mathbf{x}_0}{\sqrt{1 - \alpha_t}}, \mathbf{0}\right). \quad (6)$$

In the reverse process, DDIM first predicts \mathbf{x}_0 given \mathbf{x}_t :

$$f_\theta(\mathbf{x}_t, t) = (\mathbf{x}_t - \sqrt{1 - \alpha_t} \cdot \epsilon_\theta(\mathbf{x}_t, t)) / \sqrt{\alpha_t}, \quad (7)$$

and the reverse process is given by replacing \mathbf{x}_0 with $f_\theta(\mathbf{x}_t, t)$ in Eq. (6):

$$\mathbf{x}_{t-1} = \sqrt{\alpha_{t-1}} \left(\frac{\mathbf{x}_t - \sqrt{1 - \alpha_t} \epsilon_\theta(\mathbf{x}_t, t)}{\sqrt{\alpha_t}} \right) + \sqrt{1 - \alpha_{t-1}} \epsilon_\theta(\mathbf{x}_t, t). \quad (8)$$

We can think of DDIM as an *image encoder*, where we can run the generative process backward deterministically to obtain a noise map \mathbf{x}_T that serves as a latent variable representing \mathbf{x}_0 , as well as an *image decoder*, where we run the generative process (Eq. (8)) to decoder \mathbf{x}_0 from \mathbf{x}_T .

4. DiffProtect

4.1. Problem Formulation

In this section, we formulate the problem of adversarial attacks on face recognition systems. Suppose the face images $\mathbf{I} \in \mathcal{I} := \mathbb{R}^{H \times W \times C}$ are drawn from an underlying distribution $\mathbb{P}_{\mathcal{I}}$, where H , W and C are the height, width and the number of channels of the image respectively. Let $h(\mathbf{I}) : \mathcal{I} \rightarrow \mathbb{R}^d$ denote a face recognition model which maps an input face image in \mathcal{I} to a feature vector in \mathbb{R}^d . An *accurate* FR system can map two images \mathbf{I}_1 and \mathbf{I}_2 of the same identity to features that are close in the feature space, and to features that are far away when they are of different identities, *i.e.*, $\mathcal{D}(h(\mathbf{I}_1), h(\mathbf{I}_2)) \leq \tau$ when $y_1 = y_2$ and $\mathcal{D}(h(\mathbf{I}_1), h(\mathbf{I}_2)) > \tau$ when $y_1 \neq y_2$, where \mathcal{D} is a distance function, τ is a threshold and y_1, y_2 are the identity of \mathbf{I}_1 and \mathbf{I}_2 respectively.

In the untargeted attack or ‘‘dodging attack’’ setting, a successful attack fools the face recognition system to map an adversarial image \mathbf{I}_{adv} with the same identity as \mathbf{I} to a feature that is far away from $h(\mathbf{I})$, *i.e.*, $\mathcal{D}(h(\mathbf{I}), h(\mathbf{I}_{\text{adv}})) > \tau$. In the targeted attack or ‘‘impersonation attack’’ setting, a successful attack fools the face recognition system to map an adversarial image \mathbf{I}_{adv} with the targeted identity to a feature that is close to $h(\mathbf{I})$, *i.e.* $\mathcal{D}(h(\mathbf{I}), h(\mathbf{I}_{\text{adv}})) \leq \tau$. In this work, we focus on targeted attack setting following previous work [61, 38, 20].

4.2. Detailed Construction

The overall pipeline of DiffProtect is shown in Fig. 2. DiffProtect consists of a semantic encoder and a conditional DDIM that serves as a stochastic encoder and an image de-

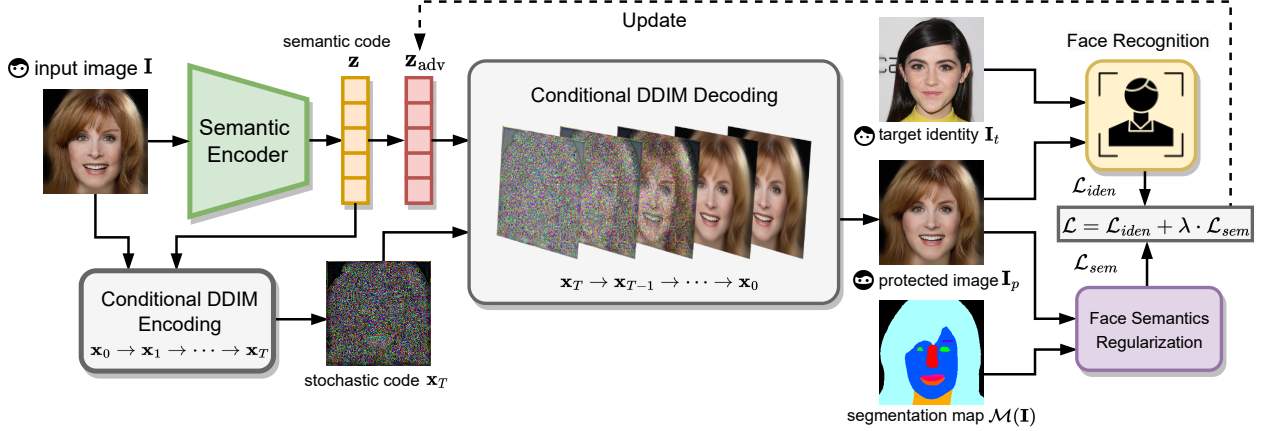


Figure 2: Overview of DiffProtect. DiffProtect utilizes a diffusion autoencoder [37], which encodes the input image as a semantic code \mathbf{z} and a stochastic code \mathbf{x}_T . We iteratively optimize an adversarial semantic code \mathbf{z}_{adv} such that the resulting protected image \mathbf{I}^p generated by the conditional DDIM decoding process can fool the face recognition model.

coder. An input face image is first encoded as a high-level semantic code \mathbf{z} and a stochastic code \mathbf{x}_T that captures low-level variations. We aim to optimize an adversarial semantic code \mathbf{z}_{adv} such that the resulting protected image \mathbf{I}_p generated by the conditional DDIM decoding process [37, 50] can fool the face recognition model to protect facial privacy.

Semantic Encoder The semantic encoder learns to map an input face image \mathbf{I} into a semantic latent code $\mathbf{z} = Enc(\mathbf{I})$ that captures high-level face semantics. Manipulating \mathbf{z} results in semantic changes in the image.

Conditional DDIM The conditional DDIM [37] is a DDIM model conditioned on the semantic code \mathbf{z} , where we train a noise prediction network $\epsilon_\theta(\mathbf{x}_t, t, \mathbf{z})$ with \mathbf{z} as an additional input. During the decoding process, we obtain the reconstructed image $\mathbf{I} = \mathbf{x}_0 = DDIM_{dec}(\mathbf{x}_T, \mathbf{z})$, by running the following deterministic generative process:

$$p_\theta(\mathbf{x}_{t-1}|\mathbf{x}_t, \mathbf{z}) = \begin{cases} \mathcal{N}(f_\theta(\mathbf{x}_1, 1, \mathbf{z}), \mathbf{0}) & \text{if } t = 1 \\ q(\mathbf{x}_{t-1}|\mathbf{x}_t, f_\theta(\mathbf{x}_t, t, \mathbf{z})) & \text{otherwise,} \end{cases} \quad (9)$$

where $f_\theta(\mathbf{x}_t, t, \mathbf{z}) = (\mathbf{x}_t - \sqrt{1 - \alpha_t} \cdot \epsilon_\theta(\mathbf{x}_t, t, \mathbf{z})) / \sqrt{\alpha_t}$, and $q(\cdot|\cdot, \cdot)$ is defined in Eq. (6).

During the encoding process, we obtain the stochastic code of the input image $\mathbf{x}_T = DDIM_{enc}(\mathbf{I}, \mathbf{z})$ by running the deterministic generative process backward:

$$\mathbf{x}_{t+1} = \sqrt{\alpha_{t+1}} f_\theta(\mathbf{x}_t, t, \mathbf{z}) + \sqrt{1 - \alpha_{t+1}} \epsilon_\theta(\mathbf{x}_t, t, \mathbf{z}). \quad (10)$$

\mathbf{x}_T is encouraged to encode only the information left out by \mathbf{z} , *i.e.*, the stochastic details.

Attack Formulation To generate a protected image \mathbf{I}_p that can effectively fool the face recognition systems and has a high visual quality to human eyes, we perturb the semantic code \mathbf{z} of the input image \mathbf{I} to obtain an adversarial

semantic code \mathbf{z}_{adv} to create semantically meaningful perturbations. We then generate \mathbf{I}_p by feeding \mathbf{z}_{adv} and \mathbf{x}_T to the DDIM decoding process:

$$\mathbf{I}_p = DDIM_{dec}(\mathbf{x}_T, \mathbf{z}_{adv}). \quad (11)$$

In this way, we constrain \mathbf{I}_p to lie on the manifold of real image distribution to ensure that \mathbf{I}_p has high visual quality.

Formally, for targeted privacy protection, we aim to solve the following optimization problem:

$$\min_{\mathbf{z}_{adv}} \mathcal{L}_{iden}(\mathbf{I}_p) = \mathcal{D}(h(\mathbf{I}_p), h(\mathbf{I}_t)), \text{ s.t. } \|\mathbf{z}_{adv} - \mathbf{z}\|_\infty < \gamma, \quad (12)$$

where \mathbf{I}_t is the face image of the target identity, \mathbf{I}_p is the protected face image generated as Eq. (11), γ is the attack budget, \mathcal{D} is the cosine distance, h is the face recognition model. In practice, the user may not have access to h . In such a black-box attack setting, we use surrogate models $g \in \mathcal{A}_g$ to estimate the identity loss \mathcal{L}_{iden} :

$$\mathcal{L}_{iden}(\mathbf{I}_p) = \sum_{g \in \mathcal{A}_g} \mathcal{D}(g(\mathbf{I}_p), g(\mathbf{I}_t)). \quad (13)$$

Face Semantics Regularization Although the attack strength is controlled by a small attack budget γ in Eq. (12) to preserve the overall facial identity to human eyes, in some cases the protected image can have different local facial features compared to the input image in order to match the characteristics of the target image, such as the face shape in Fig. 7, which may not be desired by some users.

To regularize the face semantics of the protected image, we propose a face semantic consistency loss \mathcal{L}_{sem} that computes the similarity between the semantic maps of the protected image \mathbf{I}_p and the input image \mathbf{I} :

$$\mathcal{L}_{sem}(\mathbf{I}_p) = CE(\mathcal{M}(\mathbf{I}_p), \mathcal{M}(\mathbf{I})), \quad (14)$$

where \mathcal{M} is a face parsing network that outputs the semantic map of the input image, and CE is the cross-entropy loss.

Algorithm 1 DiffProtect

- 1: **Input:** \mathbf{I} , N , γ , η , λ , T , Enc , ϵ_θ , h or \mathcal{A}_g , \mathcal{M}
 - 2: **Output:** protected image \mathbf{I}_p
 - 3: \triangleright Image Encoding
 - 4: $\mathbf{z} = Enc(\mathbf{I})$, $\mathbf{x}_T = DDIM_{enc}(\mathbf{I}, \mathbf{z})$
 - 5: \triangleright Attack Generation
 - 6: $\mathbf{z}_{adv}^{(0)} \leftarrow \mathbf{z}$
 - 7: **for** $i = 0$ **to** $N - 1$
 - 8: $\mathbf{I}_p^{(i)} = DDIM_{dec}(\mathbf{x}_T, \mathbf{z}_{adv}^{(i)})$
 - 9: **or** $\mathbf{I}_p^{(i)} \approx f_\theta(\mathbf{x}_{t_0}, t_0, \mathbf{z}_{adv}^{(i)})$ \triangleright DiffProtect-fast
 - 10: $\mathcal{L}(\mathbf{I}_p^{(i)}) = \mathcal{L}_{iden}(\mathbf{I}_p^{(i)}) + \lambda \cdot \mathcal{L}_{sem}(\mathbf{I}_p^{(i)})$
 - 11: $\mathbf{z}_{adv}^{(i+1)} = \mathcal{P}_S \left(\mathbf{z}_{adv}^{(i)} - \eta \cdot \text{sign} \left(\nabla_{\mathbf{z}_{adv}^{(i)}} \mathcal{L}(\mathbf{I}_p^{(i)}) \right) \right)$
 - 12: **end for**
 - 13: $\mathbf{z}_{adv} \leftarrow \mathbf{z}_{adv}^{(N)}$, $\mathbf{I}_p = DDIM_{dec}(\mathbf{x}_T, \mathbf{z}_{adv})$
-

The optimization problem in Eq. (12) becomes:

$$\min_{\mathbf{z}_{adv}} \mathcal{L}(\mathbf{I}_p) = \mathcal{L}_{iden}(\mathbf{I}_p) + \lambda \cdot \mathcal{L}_{sem}(\mathbf{I}_p), \text{ s.t. } \|\mathbf{z}_{adv} - \mathbf{z}\|_\infty < \gamma, \quad (15)$$

where λ is a hyper-parameter that controls the importance of the semantic consistency term.

Attack Generation The DiffProtect algorithm is summarized in Alg. 1. We iteratively solve Eq. (15) with projected gradient descent [33]:

$$\begin{cases} \mathbf{I}_p^{(i)} = DDIM_{dec}(\mathbf{x}_T, \mathbf{z}_{adv}^{(i)}) & (16) \\ \mathbf{z}_{adv}^{(i+1)} = \mathcal{P}_S \left(\mathbf{z}_{adv}^{(i)} - \eta \cdot \text{sign} \left(\nabla_{\mathbf{z}_{adv}^{(i)}} \mathcal{L}(\mathbf{I}_p^{(i)}) \right) \right) & (17) \end{cases}$$

where $\mathbf{z}_{adv}^{(0)} = \mathbf{z}$, η is the attack step size, \mathcal{P}_S is the projection onto feasible set $\mathcal{S} = \{\mathbf{z}_{adv} : \|\mathbf{z}_{adv} - \mathbf{z}\|_\infty < \gamma\}$. Note that the DDIM decoding process is fully differentiable (Eq. (9)) so we can directly compute $\nabla_{\mathbf{z}_{adv}} \mathcal{L}(\mathbf{I}_p)$ to update \mathbf{z}_{adv} .

Attack Acceleration In Eq. (16), we need to run the full DDIM decoding process to obtain $\mathbf{I}_p^{(i)}$ at each attack iteration. The time complexity for generating a protected image is $\mathcal{O}(T \times N)$, where T is the number of generative steps in the DDIM decoding process, N is the number of attack steps. To accelerate attack generation, we can instead compute an approximated version of $\mathbf{I}_p^{(i)}$ at each attack iteration by running only one generative step. Specifically, let t_0 be the time stamp from which we run the generative step to estimate $\mathbf{I}_p^{(i)}$. We can obtain the corresponding noise map \mathbf{x}_{t_0} from the DDIM encoding process and estimate $\mathbf{I}_p^{(i)}$ by:

$$\mathbf{I}_p^{(i)} \approx f_\theta(\mathbf{x}_{t_0}, t_0, \mathbf{z}_{adv}^{(i)}) = \frac{1}{\sqrt{\alpha_{t_0}}} (\mathbf{x}_{t_0} - \sqrt{1 - \alpha_{t_0}} \cdot \epsilon_\theta(\mathbf{x}_{t_0}, t_0, \mathbf{z}_{adv}^{(i)})). \quad (18)$$

In this way, we can reduce the time complexity to $\mathcal{O}(N)$. We denote this accelerated version of DiffProtect as DiffProtect-fast. Note that \mathbf{x}_{t_0} is not updated during the

attack. This simple strategy works surprisingly well as we will show in Sec. 5.2. The effect of the choice of t_0 is shown in the supplementary materials.

5. Experiments

5.1. Experimental Settings

Dataset We evaluate DiffProtect on two commonly used high-quality face image datasets: CelebA-HQ [23] and FFHQ [25]. Following [20], we use a subset of 1000 face images with different identities for each dataset.

Attack Setting In this paper, we focus on black-box targeted attacks following previous work [61, 38, 20]. We consider three popular face recognition models, including IR152 [14], IRSE50 [19], and MobileFace [5] as the victim models. For each model, we use the other models as the surrogate models \mathcal{A}_g to craft black-box attacks.

Evaluation Metrics We use Attack Success Rate (ASR) [20, 61] to evaluate the attack performance:

$$\text{ASR} = \frac{1}{K} \sum_{\mathbf{I}} \mathbb{I}(\cos(h(\mathbf{I}_t), h(\mathbf{I}_p)) > \tau) \times 100\%, \quad (19)$$

where \mathbb{I} is the indicator function, K is the number of face image \mathbf{I} , τ is the threshold, \mathbf{I}_t and \mathbf{I}_p are the target and protected face images respectively. The value of τ is set at 0.01 False Acceptance Rate (FAR) for each victim model. In addition, we use Frechet Inception Distance (FID) [16] to evaluate the naturalness of protected face images.

Implementation Details The architecture of DiffProtect is mainly based on Diffusion Autoencoder (DiffAE) [37]. We use the DiffAE model trained on the FFHQ dataset with 256×256 image resolutions. The DiffAE model is fixed during attack generation. For face semantics regularization, we use a pretrained BiSeNet [60] trained on the CelebAMask-HQ dataset [28] as the face parsing network \mathcal{M} . We set $N = 50$, $\gamma = 0.03$, $\eta = 2 \cdot \frac{\gamma}{N}$ and $\lambda = 0$ by default. We set $T = 100$ for conditional DDIM encoding and final decoding, but use five decoding steps for reconstructing $\mathbf{I}_p^{(i)}$ during attack (Eq. (16)) in order to save time and memory. For DiffProtect-fast, we set $t_0 = 60$. All experiments were run on a server with 8 Nvidia A5000 GPUs.

5.2. Comparison with the state-of-the-art

Main Results We compare DiffProtect with state-of-the-art face encryption methods, including PGD [33], MIM [7], TIP-IM [58], and AMT-GAN [20]. The implementation details of baseline methods can be found in the supplementary materials. Table 1 reports the quantitative results on the CelebA-HQ and FFHQ datasets. For ASR, DiffProtect significantly outperforms previous methods by a large

Methods	Target-specific	Natural-looking	CelebA-HQ				FFHQ			
			ASR (%) \uparrow			FID \downarrow	ASR (%) \uparrow			FID \downarrow
			IRSE50	IR152	MobileFace		IRSE50	IR152	MobileFace	
No attack	\times	\checkmark	7.3	3.8	1.1	0	4.4	2.5	5.2	0
PGD [33]	\times	\times	32.6	19.0	35.6	39.6	20.1	14.4	18.8	38.1
MIM [7]	\times	\times	37.4	31.0	35.5	69.9	24.5	23.2	21.4	62.1
TIP-IM [58]	\times	\times	47.2	35.3	45.3	71.6	31.0	27.5	26.9	62.8
AMT-GAN [20]	\checkmark	\checkmark	53.9	41.9	60.0	31.1	32.6	30.5	29.9	30.5
DiffProtect-fast ($\lambda = 0$)	\times	\checkmark	<u>68.4</u>	<u>49.8</u>	<u>72.1</u>	<u>26.7</u>	<u>50.8</u>	<u>47.6</u>	<u>47.0</u>	26.4
DiffProtect ($\lambda = 0$)	\times	\checkmark	78.4	60.3	77.9	27.6	57.7	54.3	52.9	<u>26.1</u>
DiffProtect ($\lambda = 0.2$)	\times	\checkmark	67.7	48.7	69.3	24.4	46.2	45.4	44.3	23.5

Table 1: Comparison with state-of-the-art methods on CelebA-HQ and FFHQ datasets for targeted black-box attacks. The best performance is in **bold** and the second best is underlined.



Figure 3: Visualizations of the protected face images generated by different face encryption methods on CelebA-HQ.

margin. In addition, DiffProtect achieves the lowest FID scores, which indicates that the encrypted images generated by DiffProtect are the most natural. We show some examples of protected face images in Fig. 3 with $\lambda = 0$. We can observe that DiffProtect produces good-looking protected images with natural and inconspicuous changes to the input images, such as slight changes in facial expressions. It

works well across genders, ages, and races, and in some cases even makes the images look more attractive. Compared to TIP-IM, the protected face images generated by DiffProtect have no obvious noise pattern as we only perturb the semantic codes and generate the images through a conditional DDIM. Compared to AMT-GAN, DiffProtect can better preserve image styles and details and does

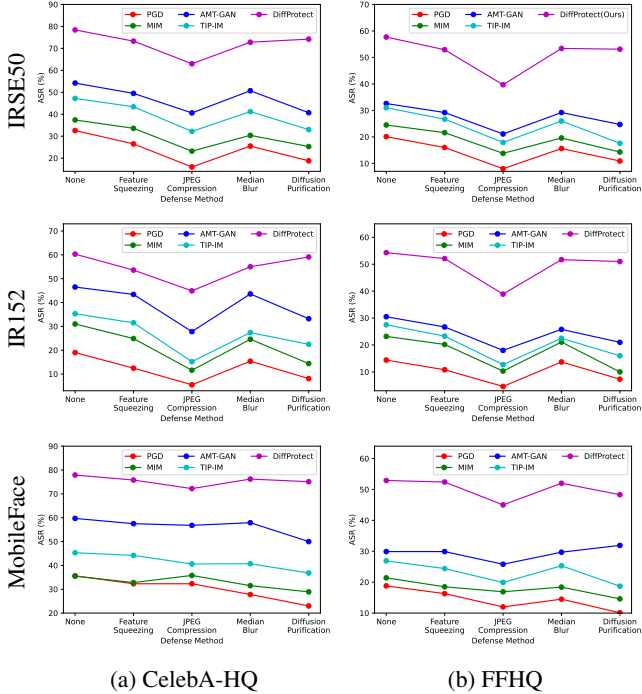


Figure 4: ASR under various defense methods.

not require training a target-specific model for each identity. Our accelerated method DiffProtect-fast also achieves higher ASRs and lower FID compared to the baselines. In addition, we can observe that DiffProtect and DiffProtect-fast achieve similar visual quality, while DiffProtect-fast requires 50% less computation time (more details in the supplementary material).

ASR under Defenses We further evaluate the effectiveness of DiffProtect against four adversarial defense methods, including feature squeezing [57], median blurring [29], JPEG compression [8], and a state-of-the-art diffusion-based defense DiffPure [36]. The implementation details of the defenses can be found in the supplementary materials. From Fig. 4 we can see that DiffProtect still achieves higher ASR under various defenses. In addition, DiffProtect is much more resilient to the DiffPure defense compared to baseline methods since it generates semantically meaningful perturbations to the input images that are hard to remove during the diffusion denoising process of DiffPure.

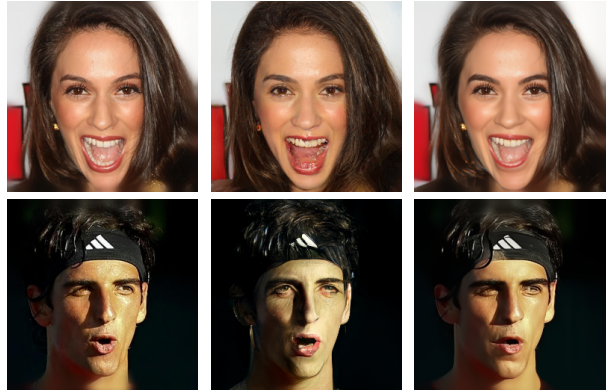
5.3. Ablation Studies

For ablation studies, we use the CelebA dataset and MobileFace as the victim model. We set $N = 10$, $\gamma = 0.02$, and $T = 50$. The other settings are the same as Sec. 5.1.

GAN vs. Diffusion model To have a fair comparison between GAN-based and Diffusion-based methods,

Dataset	Model	IRSE50	IR152	MobileFace
CelebA-HQ	GAN	33.0	16.5	41.1
	Diff.	60.7 (+27.7)	37.5 (+21.0)	62.0 (+20.6)
FFHQ	GAN	21.3	20.0	21.2
	Diff.	36.5 (+15.2)	33.1 (+13.1)	34.0 (+12.8)

Table 2: ASR (%) of GAN [53] and Diffusion [37] model.



(a) Input image (b) GAN output. (c) Diffusion output.

Figure 5: Visualizations of adversarial images generated by GAN [53] and diffusion [37] models on CelebA-HQ.

we re-implement our method using a GAN-based autoencoder [53] where we also iteratively optimize the GAN latent code using the same formulation. The implementation details can be found in the supplementary materials. The results are summarized in Table 2. We can observe that the diffusion-based method has much higher ASRs than the GAN-based method. From Fig. 5 we can observe that the image quality of Diffusion model output is also visually better than the GAN-based method. These results confirm our intuition that a better generative model like a Diffusion model can help to improve both attack performance and image quality.

Effect of Attack Budget We show the effect of attack budget γ in Fig. 6. We can observe that as γ increases, the ASR also increases; when $\gamma = 0$, we have $ASR = 97.7\%$. However, the FID also goes up as γ increases, which indicates that the image quality becomes worse. In addition, a large γ can cause the protected image to lose the visual identity of the input image. In practice, we recommend setting $\gamma \leq 0.03$ such that the output images have high visual quality and preserve the identity of the input images, which is confirmed by a user study using Amazon Mechanical Turk (see the supplementary material).

Effect of Face Semantics Regularization We show the effect of face semantics regularization in Fig. 7. Without the face semantics regularization term ($\lambda = 0$), the protected

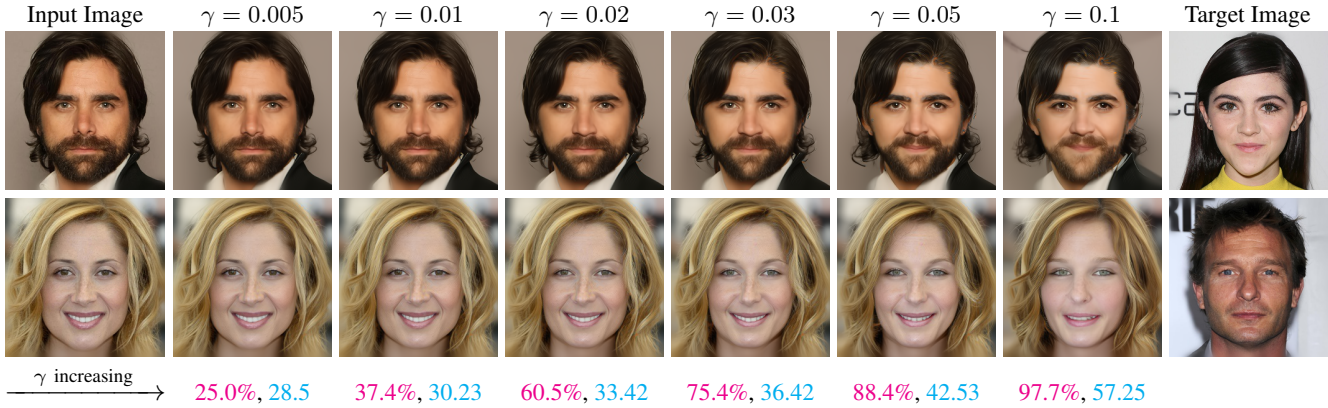


Figure 6: Visual comparisons of different attack budget γ and the corresponding ASR and FID.

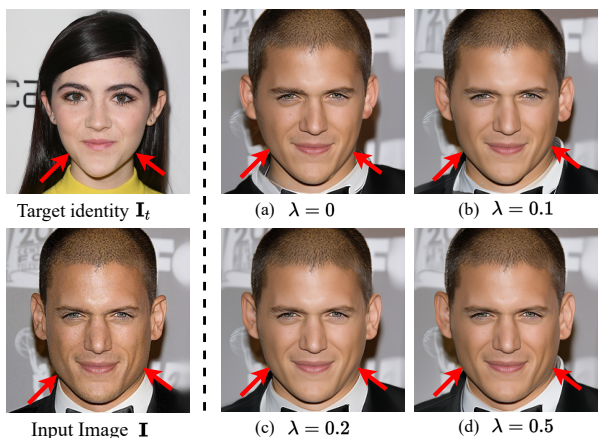


Figure 7: Effect of Face Semantics Regularization. (a)-(d): protected image I_p generated with different λ in Eq. (15). Increasing λ gradually changes the face shape from a heart shape (similar to I_t) to a square shape (similar to I).

λ	0	0.01	0.05	0.1	0.2	0.5
ASR (%) \uparrow	60.5	60.3	58.9	56.3	53.5	46.1
FID \downarrow	33.4	33.3	32.8	32.4	31.9	31.2

Table 3: Quantitative results of face semantics regularization with different λ in Eq. (15).

image can have different local facial features compared to the input image to match the characteristics of the target image, such as the face shape in Fig. 7 (a). Increasing the value of λ helps to preserve the face features of the input images. Quantitatively, from Table 3 we can observe that increasing λ helps to reduce FID, which indicates better image quality but also decreases ASR. In practice, a user can choose a value of λ as well as the attack budget γ depending on their own preference.

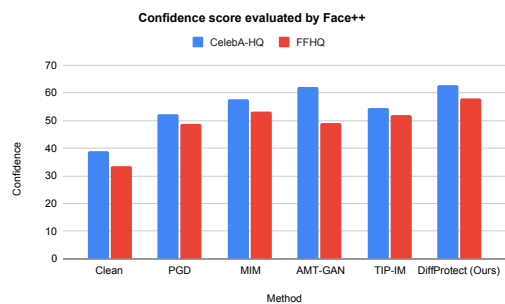


Figure 8: Confidence scores of different methods evaluated by commercial API Face++.

5.4. Evaluation on Commercial API

We further evaluate the effectiveness of AGE-FTM in the real world using a commercial FR API Face++¹, where we compute the confidence scores between the protected images and the target identity image. DiffProtect achieves average confidence scores of 62.8% and 58.03% for CelebA-HQ and FFHQ respectively, which are higher than baseline methods. This shows that the proposed method has a satisfactory attack ability even for the commercial API while achieving good image quality.

6. Conclusion

In this work, we propose DiffProtect a novel diffusion-based method for facial privacy protection. It generates semantically meaningful perturbations to the input images and produces adversarial images of high visual quality. Our extensive experiments on CelebA-HQ and FFHQ demonstrate that DiffProtect significantly outperforms previous state-of-the-art methods for both attack performance and image quality.

¹<https://www.faceplusplus.com/>

References

- [1] Nicholas Carlini, J Zico Kolter, Florian Tramèr, Krishnamurthy Dvijotham, Leslie Rice, and Mingjie Sun. (certified!) adversarial robustness for free! In *ICLR*, 2023. **2**
- [2] Nicholas Carlini and David Wagner. Towards evaluating the robustness of neural networks. In *IEEE Symposium on Security and Privacy (SP)*, 2017. **2**
- [3] Valeriia Cherepanova, Micah Goldblum, Harrison Foley, Shiyuan Duan, John Dickerson, Gavin Taylor, and Tom Goldstein. Lowkey: Leveraging adversarial attacks to protect social media users from facial recognition. In *ICLR*, 2021. **1, 2, 3**
- [4] Yunjey Choi, Minje Choi, Munyoung Kim, Jung-Woo Ha, Sunghun Kim, and Jaegul Choo. StarGAN: Unified Generative Adversarial Networks for Multi-Domain Image-to-Image Translation. In *CVPR*, 2018. **1**
- [5] Jiankang Deng, Jia Guo, Niannan Xue, and Stefanos Zafeiriou. Arcface: Additive angular margin loss for deep face recognition. In *CVPR*, 2019. **1, 5**
- [6] Prafulla Dhariwal and Alexander Nichol. Diffusion models beat gans on image synthesis. In *NeurIPS*, 2021. **2**
- [7] Yinpeng Dong, Fangzhou Liao, Tianyu Pang, Hang Su, Jun Zhu, Xiaolin Hu, and Jianguo Li. Boosting adversarial attacks with momentum. In *CVPR*, 2018. **2, 5, 6, 11**
- [8] Gintare Karolina Dziugaite, Zoubin Ghahramani, and Daniel M Roy. A study of the effect of jpg compression on adversarial images. *arXiv preprint arXiv:1608.00853*, 2016. **7**
- [9] Gintare Karolina Dziugaite, Zoubin Ghahramani, and Daniel M Roy. A study of the effect of jpg compression on adversarial images. *arXiv preprint arXiv:1608.00853*, 2016. **11**
- [10] Ian Goodfellow, Jean Pouget-Abadie, Mehdi Mirza, Bing Xu, David Warde-Farley, Sherjil Ozair, Aaron Courville, and Yoshua Bengio. Generative adversarial nets. In *NeurIPS*, 2014. **1**
- [11] Ian J Goodfellow, Jonathon Shlens, and Christian Szegedy. Explaining and harnessing adversarial examples. In *ICLR*, 2015. **2**
- [12] Sven Gowal, Sylvester-Alvise Rebuffi, Olivia Wiles, Florian Stimberg, Dan A. Calian, and Timothy Mann. Improving robustness using generated data. *arXiv preprint arXiv:2110.09468*, 2021. **2**
- [13] Shuangchi Gu, Ping Yi, Ting Zhu, Yao Yao, and Wei Wang. Detecting adversarial examples in deep neural networks using normalizing filters. *UMBC Student Collection*, 2019. **11**
- [14] Kaiming He, Xiangyu Zhang, Shaoqing Ren, and Jian Sun. Deep residual learning for image recognition. In *Proceedings of the IEEE conference on computer vision and pattern recognition*, pages 770–778, 2016. **5**
- [15] Yonghao He, Dezhong Xu, Lifang Wu, Meng Jian, Shiming Xiang, and Chunhong Pan. LFFD: A light and fast face detector for edge devices. *arXiv preprint arXiv:1904.10633*, 2019. **1**
- [16] Martin Heusel, Hubert Ramsauer, Thomas Unterthiner, Bernhard Nessler, and Sepp Hochreiter. Gans trained by a two time-scale update rule converge to a local nash equilibrium. *Advances in neural information processing systems*, 30, 2017. **5**
- [17] Kashmir Hill. The secretive company that might end privacy as we know it. In *Ethics of Data and Analytics*, pages 170–177. Auerbach Publications, 2020. **1**
- [18] Jonathan Ho, Ajay Jain, and Pieter Abbeel. Denoising diffusion probabilistic models. *NeurIPS*, 2020. **2, 3**
- [19] Jie Hu, Li Shen, and Gang Sun. Squeeze-and-excitation networks. In *CVPR*, 2018. **2, 5**
- [20] Shengshan Hu, Xiaogeng Liu, Yechao Zhang, Minghui Li, Leo Yu Zhang, Hai Jin, and Libing Wu. Protecting facial privacy: Generating adversarial identity masks via style-robust makeup transfer. In *CVPR*, 2022. **1, 2, 3, 5, 6, 11, 13, 14**
- [21] Ajil Jalal, Andrew Ilyas, Constantinos Daskalakis, and Alexandros G Dimakis. The robust manifold defense: Adversarial training using generative models. *arXiv preprint arXiv:1712.09196*, 2017. **2**
- [22] Shuai Jia, Bangjie Yin, Taiping Yao, Shouhong Ding, Chunhua Shen, Xiaokang Yang, and Chao Ma. Adv-Attribute: Inconspicuous and Transferable Adversarial Attack on Face Recognition. In *NeurIPS*, 2022. **1, 3**
- [23] Tero Karras, Timo Aila, Samuli Laine, and Jaakko Lehtinen. Progressive growing of GANs for improved quality, stability, and variation. In *ICLR*, 2018. **2, 5**
- [24] Tero Karras, Miika Aittala, Timo Aila, and Samuli Laine. Elucidating the design space of diffusion-based generative models. In *NeurIPS*, 2022. **2**
- [25] Tero Karras, Samuli Laine, and Timo Aila. A style-based generator architecture for generative adversarial networks. In *CVPR*, 2019. **1, 2, 5**
- [26] Diederik P. Kingma and Max Welling. Auto-encoding variational bayes. In *ICLR*, 2014. **2**
- [27] Stepan Komkov and Aleksandr Petiushko. AdvHat: Real-world adversarial attack on ArcFace face ID system. In *ICPR*, 2021. **1, 2, 3**
- [28] Cheng-Han Lee, Ziwei Liu, Lingyun Wu, and Ping Luo. MaskGAN: Towards Diverse and Interactive Facial Image Manipulation. In *CVPR*, 2020. **5**
- [29] Xin Li and Fuxin Li. Adversarial examples detection in deep networks with convolutional filter statistics. In *ICCV*, 2017. **7**
- [30] Xin Li and Fuxin Li. Adversarial examples detection in deep networks with convolutional filter statistics. In *Proceedings of the IEEE international conference on computer vision*, pages 5764–5772, 2017. **11**
- [31] Wei-An Lin, Chun Pong Lau, Alexander Levine, Rama Chellappa, and Soheil Feizi. Dual Manifold Adversarial Robustness: Defense against Lp and non-Lp Adversarial Attacks. In *NeurIPS*, 2020. **2**
- [32] Taylor Kay Lively. Facial recognition in the US: Privacy concerns and legal developments. rb.gy/u8i6ny. Accessed: 2/14/2023. **1**
- [33] Aleksander Madry, Aleksandar Makelov, Ludwig Schmidt, Dimitris Tsipras, and Adrian Vladu. Towards deep learning models resistant to adversarial attacks. In *ICLR*, 2018. **2, 5, 6, 11**

- [34] Paul Mozur and Aaron Krolik. A surveillance net blankets China’s cities, giving police vast powers. *The New York Times*, 17, 2019. 1
- [35] Alexander Quinn Nichol and Prafulla Dhariwal. Improved denoising diffusion probabilistic models. In *ICML*, 2021. 2, 3
- [36] Weili Nie, Brandon Guo, Yujia Huang, Chaowei Xiao, Arash Vahdat, and Anima Anandkumar. Diffusion models for adversarial purification. In *ICML*, 2022. 2, 7, 11
- [37] Konpat Preechakul, Nattanat Chatthee, Suttisak Widadwongsa, and Supasorn Suwajanakorn. Diffusion autoencoders: Toward a meaningful and decodable representation. In *CVPR*, 2022. 2, 4, 5, 7
- [38] Haonan Qiu, Chaowei Xiao, Lei Yang, Xinchen Yan, Honglak Lee, and Bo Li. Semanticadv: Generating adversarial examples via attribute-conditioned image editing. In *ECCV*, 2020. 1, 2, 3, 5
- [39] Sylvestre-Alvise Rebuffi, Sven Gowal, Dan A. Calian, Florian Stimberg, Olivia Wiles, and Timothy Mann. Fixing data augmentation to improve adversarial robustness. *arXiv preprint arXiv:2103.01946*, 2021. 2
- [40] Robin Rombach, Andreas Blattmann, Dominik Lorenz, Patrick Esser, and Björn Ommer. High-resolution image synthesis with latent diffusion models. In *CVPR*, 2022. 2
- [41] Olaf Ronneberger, Philipp Fischer, and Thomas Brox. U-Net: Convolutional networks for biomedical image segmentation. In *MICCAI*, 2015. 3
- [42] ADAM SATARIANO. Police use of facial recognition is accepted by british court. *The New York Times*, 4, 2019. 1
- [43] Florian Schroff, Dmitry Kalenichenko, and James Philbin. FaceNet: A unified embedding for face recognition and clustering. In *CVPR*, 2015. 1
- [44] Shawn Shan, Emily Wenger, Jiayun Zhang, Huiying Li, Haitao Zheng, and Ben Y Zhao. Fawkes: Protecting privacy against unauthorized deep learning models. In *29th USENIX Security Symposium (USENIX Security 20)*, pages 1589–1604, 2020. 2
- [45] Mahmood Sharif, Sruti Bhagavatula, Lujo Bauer, and Michael K Reiter. A general framework for adversarial examples with objectives. *ACM Transactions on Privacy and Security (TOPS)*, 22(3):1–30, 2019. 1, 2, 3
- [46] Yan Shoshitaishvili, Christopher Kruegel, and Giovanni Vigna. Portrait of a Privacy Invasion. *Proceedings on Privacy Enhancing Technologies*, 2015(1):41–60, 2015. 1
- [47] Maya Shwayder. Clearview ai’s facial-recognition app is a nightmare for stalking victims. *Digital Trends*, 2020. 1
- [48] Jascha Sohl-Dickstein, Eric Weiss, Niru Maheswaranathan, and Surya Ganguli. Deep unsupervised learning using nonequilibrium thermodynamics. In *ICML*, 2015. 2, 3
- [49] Kihyuk Sohn, Honglak Lee, and Xinchen Yan. Learning structured output representation using deep conditional generative models. In *NeurIPS*, 2015. 2
- [50] Jiaming Song, Chenlin Meng, and Stefano Ermon. Denoising diffusion implicit models. In *ICLR*, 2021. 2, 3, 4
- [51] Yang Song, Jascha Sohl-Dickstein, Diederik P Kingma, Abhishek Kumar, Stefano Ermon, and Ben Poole. Score-based generative modeling through stochastic differential equations. *arXiv preprint arXiv:2011.13456*, 2020. 2
- [52] David Stutz, Matthias Hein, and Bernt Schiele. Disentangling adversarial robustness and generalization. In *CVPR*, 2019. 2
- [53] Tengfei Wang, Yong Zhang, Yanbo Fan, Jue Wang, and Qifeng Chen. High-fidelity GAN inversion for image attribute editing. In *CVPR*, 2022. 7, 11
- [54] Zekai Wang, Tianyu Pang, Chao Du, Min Lin, Weiwei Liu, and Shuicheng Yan. Better diffusion models further improve adversarial training. *arXiv preprint arXiv:2302.04638*, 2023. 2
- [55] Eric Wong and J Zico Kolter. Learning perturbation sets for robust machine learning. In *ICLR*, 2021. 2
- [56] Chaowei Xiao, Bo Li, Jun-Yan Zhu, Warren He, Mingyan Liu, and Dawn Song. Generating adversarial examples with adversarial networks. In *IJCAI*, 2018. 2
- [57] Weilin Xu, David Evans, and Yanjun Qi. Feature squeezing: Detecting adversarial examples in deep neural networks. *arXiv preprint arXiv:1704.01155*, 2017. 7
- [58] Xiao Yang, Yinpeng Dong, Tianyu Pang, Hang Su, Jun Zhu, Yuefeng Chen, and Hui Xue. Towards face encryption by generating adversarial identity masks. In *CVPR*, 2021. 1, 2, 3, 5, 6, 11, 13, 14
- [59] Bangjie Yin, Wenxuan Wang, Taiping Yao, Junfeng Guo, Zelun Kong, Shouhong Ding, Jilin Li, and Cong Liu. Adv-Makeup: A New Imperceptible and Transferable Attack on Face Recognition. *arXiv preprint arXiv:2105.03162*, 2021. 1, 2, 3
- [60] Changqian Yu, Jingbo Wang, Chao Peng, Changxin Gao, Gang Yu, and Nong Sang. BiSeNet: Bilateral segmentation network for real-time semantic segmentation. In *ECCV*, 2018. 5
- [61] Yaoyao Zhong and Weihong Deng. Towards transferable adversarial attack against deep face recognition. *IEEE Transactions on Information Forensics and Security*, 16:1452–1466, 2020. 1, 3, 5

Supplementary Material

A. DiffProtect-fast

A.1. Effect of t_0

In DiffProtect-fast, we run one generative step from the time stamp t_0 to compute $\mathbf{I}_p^{(i)}$, instead of running the whole generative process from $t = T$ to $t = 0$ to accelerate attack generation. We show the effect of the choice of t_0 in Fig. 9, where we use the same settings as in the ablation studies. We can observe that when we increase t_0 , ASR first increases and then decreases, while FID first decreases and then increases, which indicates the image quality also first increases and then decreases. This shows that choosing t_0 at the early or late stage of the generative process is less effective. We set $t_0/T = 0.6$, *i.e.*, $t_0 = 0.6 \cdot T$, as this ratio achieves the highest ASR and is also a local minimum for FID.

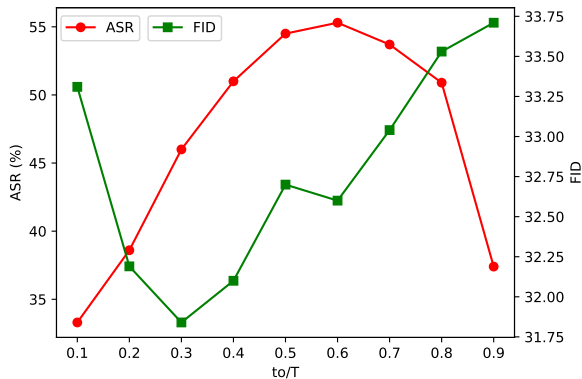


Figure 9: Effect of t_0/T ratio for DiffProtect-fast.

A.2. Comparison with DiffProtect

We provide quantitative comparisons between DiffProtect and DiffProtect-fast in Table 4. Compared to DiffProtect, DiffProtect-fast achieves lower ASRs, and similar FIDs, but requires much less computation time. Note that DiffProtect-fast also outperforms the baseline methods as shown in Table 1 of the main paper. These results demonstrate that the attack acceleration strategy is very effective and we can use DiffProtect-fast to achieve a trade-off between computation time and attack success rate. In addition, by comparing the last two rows of Figs. 10 and 11, we can observe that the protected images generated by DiffProtect and DiffProtect-fast are visually similar.

B. Additional Implementation Details

B.1. Baselines

For l_∞ attacks such as PGD [33], MIM [7] and TIP-IM [58], the attack budget is set to be $16/255$ with 100 at-

tack iterations. For MIM, the decay factor μ is set to 1.0. For TIP-IM, the gamma value for the MMD loss is set to 0 by default. For AMT-GAN [20], we use the default setting.

B.2. Defense methods

We evaluated our methods with four defense methods: feature squeezing [13], JPEG compression [9], median blur [30], and adversarial purification [36]. For feature squeezing, the bit depth is set to 3. For JPEG compression, the quality factor is set to 5. For the median blur, the kernel size is set to 7. For adversarial purification, we set the diffusion timestep to be 0.0075.

B.3. GAN-based attack

To have a fair comparison between GAN-based and Diffusion-based methods, we re-implement our method using an HFGI [53] model, a state-of-the-art method that uses a high-fidelity GAN and can invert and edit high-resolution face images effectively. HFGI consists of an encoder E to encode the images and uses a generator G to edit the high-resolution face images. To craft the GAN-based attack, we first pass the image to the encoder to get the latent code $z = E(I)$. Then we perturb z by minimizing Eq. (15) of the main paper to obtain the adversarial latent code z^{adv} . Finally, we decode z^{adv} to an adversarial image using the generator G . We set the attack budget to 0.1, with step size 0.02 in 10 iterations.

C. Additional Experimental Results

We show the effect of attack iterations in Table 5, where we change the number of attack iterations N and the other settings are the same as in the ablation studies. We can observe that as N increases, ASR also increases while FID stays relatively the same. We set $N = 50$ in our main experiments.

D. User Study

To further investigate the effect of different attack budgets for preserving facial identity, we conduct a user study using Amazon Mechanical Turk (MTurk), where we show the worker the original image \mathbf{I} and the protected image \mathbf{I}_p generated with different attack budget γ . For each pair of \mathbf{I} and \mathbf{I}_p , the worker is asked to provide a rating from 1 to 10 of “how likely the two face images belong to the same person?” with 1 being “extremely unlikely” and 10 being “extremely likely”. We randomly selected 50 images from our CelebA-HQ test set for the user study and each pair of \mathbf{I} and \mathbf{I}_p is evaluated by ten MTurk workers. The average ratings are shown in Table 6. We chose $\gamma = 0.03$ since it achieves a high user rating as well as a high ASR (78.4%) and low FID (27.6). In practice, a user can choose the value of γ themselves based on their own preferences.

Methods	CelebA-HQ					FFHQ				
	ASR (%) \uparrow			FID \downarrow	Time (s) \downarrow	ASR (%) \uparrow			FID \downarrow	Time (s) \downarrow
	IRSE50	IR152	MobileFace			IRSE50	IR152	MobileFace		
DiffProtect-fast	68.4	49.8	72.1	26.7	18.9	50.8	47.6	47.0	26.4	18.3
DiffProtect	78.4	60.3	77.9	27.6	36.4	57.7	54.3	52.9	26.1	35.9

Table 4: Comparison between DiffProtect and DiffProtect-fast.

N	2	5	10	20	50
ASR (%) \uparrow	47.3	57.2	60.5	61.9	63.1
FID \downarrow	32.4	33.3	33.4	33.6	33.7

Table 5: Effect of attack iteration N .

γ	0.005	0.01	0.02	0.03	0.05	0.1
Rating \uparrow	8.9	8.7	7.9	7.0	5.5	4.7

Table 6: Identity similarity ratings of different γ .

E. More Visualization Results

We provide more examples of protected face images in Figs. 10 and 11. We can observe that DiffProtect produces good-looking protected images with natural and inconspicuous changes to the input images, such as slight changes in facial expressions. It works well across genders, ages, and races, and in some cases even makes the images look more attractive. Compared to TIP-IM, the protected face images generated by DiffProtect have no obvious noise pattern as we only perturb the semantic codes and generate the images through a conditional DDIM. Compared to AMT-GAN, DiffProtect can better preserve image styles and details and does not require training a target-specific model for each identity.

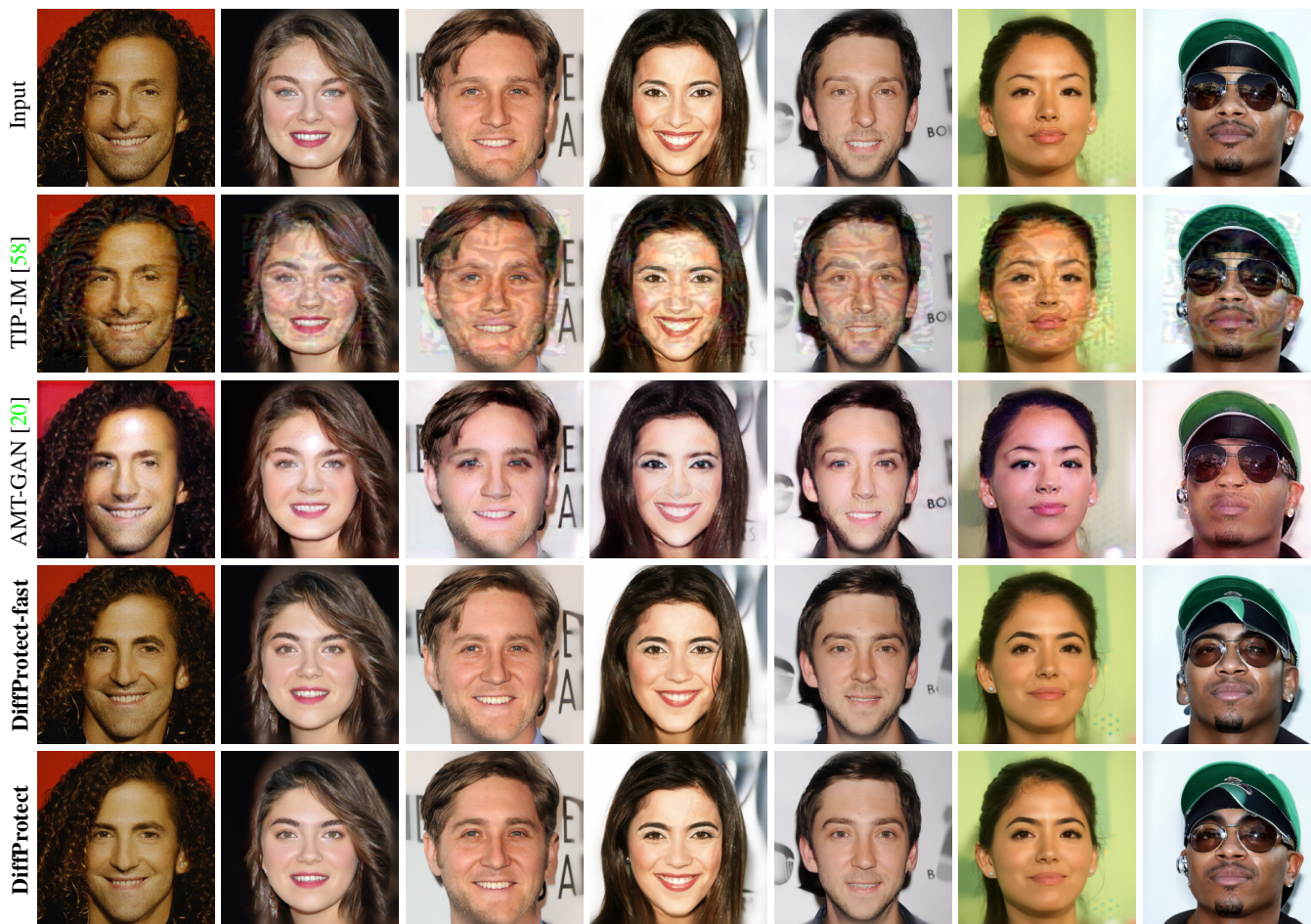


Figure 10: Visualizations of the protected face images generated by different face encryption methods on CelebA-HQ.

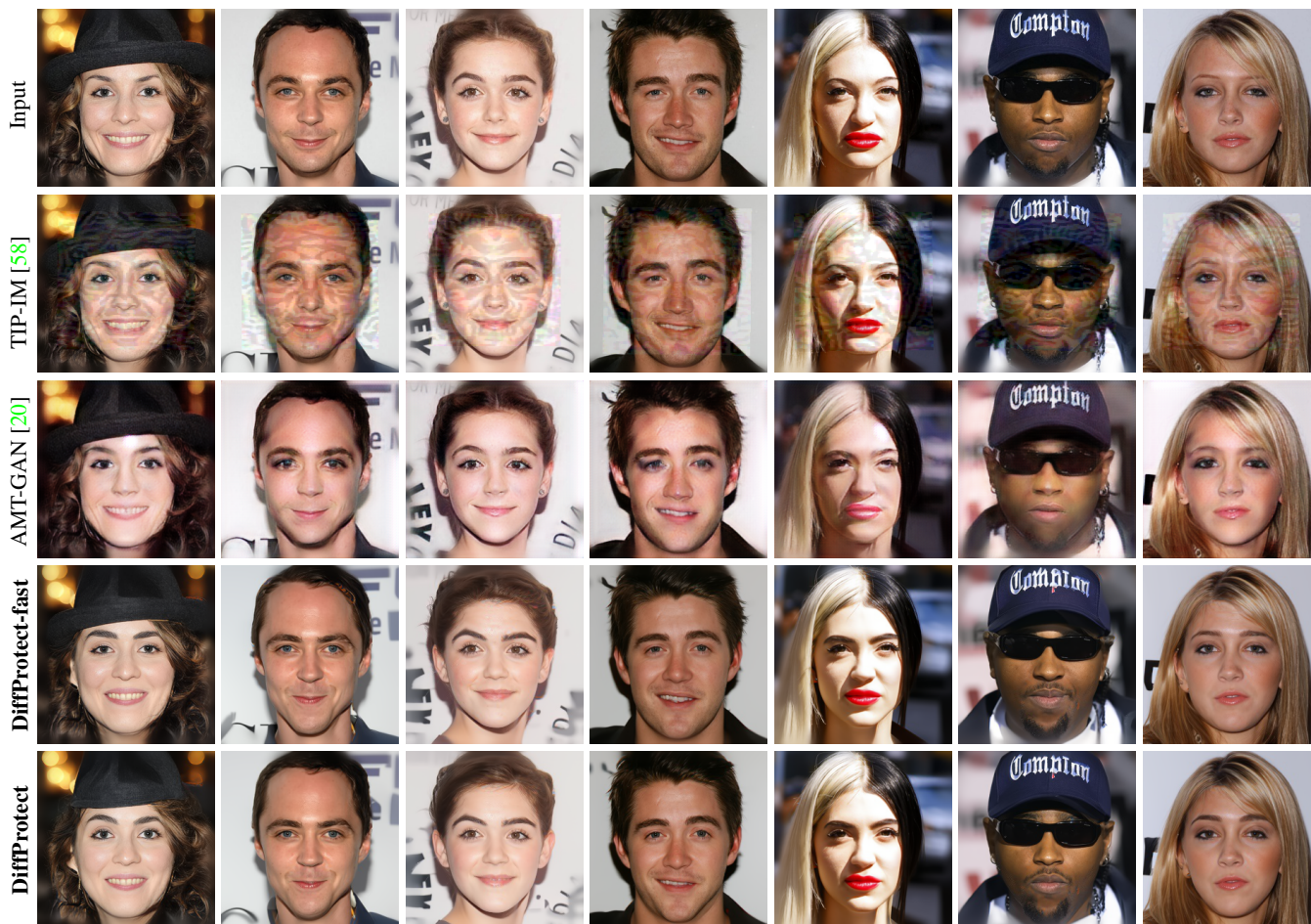


Figure 11: Visualizations of the protected face images generated by different face encryption methods on CelebA-HQ.